

**Resonance production in heavy ion collisions: Suppression of  $\Lambda(1520)$  and enhancement of  $\Sigma(1385)$** Inga Kuznetsova<sup>1</sup> and Johann Rafelski<sup>1,2</sup><sup>1</sup>*Department of Physics, University of Arizona, Tucson, Arizona 85721, USA*<sup>2</sup>*Department für Physik der Ludwig-Maximilians-Universität München and Maier-Leibnitz-Laboratorium  
Am Coulombwall 1, D-85748 Garching, Germany*

(Received 10 November 2008; published 28 January 2009)

We investigate the yield of  $\Lambda(1520)$  resonance in heavy ion collisions within the framework of a kinetic master equation without the assumption of chemical equilibrium. We show that reactions such as  $\Lambda(1520) + \pi \leftrightarrow \Sigma^*$  can favor  $\Sigma^*$  production, thereby decreasing the  $\Lambda(1520)$  yield. Within the same approach we thus find a yield enhancement for  $\Sigma(1385)$  and a yield suppression for  $\Lambda(1520)$ .

DOI: [10.1103/PhysRevC.79.014903](https://doi.org/10.1103/PhysRevC.79.014903)

PACS number(s): 25.75.Dw, 12.38.Mh, 24.10.Pa, 25.75.Nq

**I. INTRODUCTION**

Hadron resonances are observed in a surprisingly large yield when a quark-gluon plasma (QGP) fireball breaks up into hadrons [1–6]. This is unexpected, since the invariant mass signature formed from decay products could be erased by rescattering of the strongly interacting decay products [7]. Thus a direct detection of resonances implies an exceedingly short period of hadron scattering, and/or a final state repopulated by hadronic interactions [8]. As a result, the final resonance yield can be considerably different from statistical hadron gas (SHG) benchmark expectation. It has already been reported that the short lived (compared to characteristic hadron phase evolution times) resonances are in general enhanced [9] compared to SHG benchmark yield.

The new result, we obtain here, is that the long lived resonances, such as  $\Lambda(1520)$ , can be considerably suppressed in their yield. This effect is amplified for the case when the initial hadron fugacities, and thus particle yields, are above chemical equilibrium. This situation is expected for a hadronizing QGP phase. The low  $\Lambda(1520)$  yield has been reported both in RHIC and SPS experiments [1,2].

In a global QGP breakup (hadron chemical freeze-out) particles and resonances are formed. Many resonances have a relatively large decay rates. This implies a large scattering formation rate. Thus resonances are exceptionally strongly interacting particles and continue to evolve in what we call kinetic phase, even after all other particles freeze-out. This continued reaction phase is specific to the resonances and can last considerably beyond the last nonresonant (elastic) scattering.

The resonance suppression, or enhancement, mechanism works as follows. In thermal hadronic gas the reaction,



can occur in both directions: the resonance decay  $3 \rightarrow 1 + 2$ , and the back-reaction (regeneration) resonance formation  $1 + 2 \rightarrow 3$ . When the reaction goes with the same rate in both directions, we have chemical detailed balance, e.g., particles yields do not change in this period of temporal evolution of the system. This does not necessarily mean that we have a chemical equilibrium. Instead it may be a transient condition for which

none of the three particles is equilibrated chemically—we will show when this can happen.

In the study of resonance decay and regeneration we are using the momentum integrated population master equations. We assume a fireball expansion model governed by hydrodynamic inspired flow with conserved entropy content. In our considerations we presume that the yield of pions  $\pi$  is so large that we can assume it not to be materially affected by any of the reactions we consider. Thus we fix pion yield in terms of an ambient fugacity and temperature value, and in essence the total (per unit rapidity at RHIC) yield is fixed since we conserve entropy.

An important assumption implied below is that the rapidly expanding hadron system maintains for the relevant particles a fully thermal (Boltzmann) momentum distribution. To describe the evolution of hadron abundances in the kinetic phase we track in time the yields of single strange hadrons after their initial formation. This is implemented in terms of time dependence of the chemical fugacities  $\Upsilon(t)$ , and the time dependence of the hadronization temperature  $T(t)$ .

We look in detail at three potential evolution scenarios:

- (i) a high temperature breakup at  $T_0 \simeq 180$  MeV where the entropy content of the equilibrated QGP and HG-phase are similar;
- (ii) the  $T_0 \simeq 160$  MeV case where chemical nonequilibrium among produced hadrons is already required; and
- (iii) at  $T_0 \simeq 140$  MeV which is favored by descriptions of stable hadron production, and in which case a strong chemical nonequilibrium situation arises.

For the late stage of the expansion, at relatively low density the assumption of thermal momentum distribution may not be anymore fully satisfied. In particular pions of high momentum could be escaping from the fireball. For this reason we will consider here a second scenario, which we call “dead channel”. In this scenario we assume that the reaction (1) goes mainly in the direction of resonance three decay and the resonance formation is switched off for

$$m_3 - (m_1 + m_2) > 300 \text{ MeV}. \quad (2)$$

Without a complete kinetic model including equilibration and particle emission we do not know the exact energy in condition (2) and timescale (during expansion) for which

Boltzmann distribution is violated and dead channels appear. It is possible that reality lies between the two cases (kinetic Boltzmann distribution and dead-channels) considered here which, in our opinion, are the two most extreme limits.

For  $\Lambda(1520)/\Lambda^0$  ratio calculations we employ and develop further the approach used for  $\Sigma(1385)/\Lambda^0$  in [9]. However, in chapter II A we investigate many further reactions in which resonance  $\Lambda(1520)$  participates. Thus we are obliged to develop a completely numerical evolution, for which the analytical study of  $\Sigma(1385)/\Lambda^0$  provides a benchmark check of our approach. In addition to new and numerous reaction channels we also introduce deformation of the reaction rates due to stimulated Bose enhancement of the reactions. This formalism is presented in Sec. II B. We discuss the temporal evolution of HG particle fugacities  $\Upsilon(t)$  in Sec. III A. In Sec. III B we present results for the evolution of particle  $\Sigma(1385)$ ,  $\Lambda(1520)$  multiplicities during kinetic phase. In Sec. III C we obtain the observable ‘ob’ ratios  $\Lambda(1520)_{\text{ob}}/\Lambda_{\text{tot}}$  and  $\Sigma(1385)_{\text{ob}}/\Lambda_{\text{tot}}$ . We discuss our results in Sec. IV.

## II. KINETIC EQUATIONS

### A. Reactions scheme for $\Lambda(1520)$ and $\Sigma(1385)$

In Fig. 1 we show the scheme of reactions which all have a noticeable effect on  $\Lambda(1520)$  yield after the chemical freeze-out kinetic phase. The format of this presentation is inspired by nuclear reactions schemes. On the vertical axis the energy scale is shown in MeV. There are three classes of particle states, which we denote from left to right as “N” ( $S = 0$  baryon), “ $\Sigma$ ”

( $S = -1, I = 1$  hyperon), and “ $\Lambda$ ” ( $S = -1, I = 0$  hyperon). Near each particle bar we state (on-line in blue) its mass, and/or angular momentum and/or total width in MeV. The states  $\Lambda(1520)$  and  $\Sigma(1385)$  are shown along with the location in energy of  $\Lambda(1520) + \pi$  and  $\Sigma(1385) + \pi$ , respectively, both entries are connected by the curly bracket, and are highlighted (on-line in red). The inclusion of the  $\pi$ -mass is helping to see the kinetic threshold energy of a reaction. The lines connecting the N,  $\Sigma$ ,  $\Lambda$  columns are indicating the reactions we consider in the numerical computations. All reactions shown in Fig. 1 can go in both directions, as shown by the double arrows placed next to the numerical value of the partial decay width  $\Gamma_i$  in MeV.

$\Lambda(1520)$  decays with a total decay width of about 15.6 MeV, with two main channels:

$$\begin{aligned} \Sigma + \pi &\leftrightarrow \Lambda(1520), & \Gamma &\approx 6.5 \text{ MeV}; \\ N + K &\leftrightarrow \Lambda(1520), & \Gamma &\approx 7 \text{ MeV}. \end{aligned} \tag{3}$$

However,  $\Lambda(1520)$  reacts with several heavier  $\Sigma^*$ -resonances, ( $\Sigma^* \equiv \Sigma(1670), \Sigma(1750), \Sigma(1775), \Sigma(1940), \Sigma(2030)$ ):

$$\Lambda(1520) + \pi \leftrightarrow \Sigma^*, \tag{4}$$

and these reactions have a larger reaction strength shown in Fig. 1.  $\Lambda(1520)$  nearly behaves like a ‘stable’ hadronic particle since:

- (i) it is dominantly coupled to heavier resonances;
- (ii) its natural lifespan is larger than the hadronic reaction rate.

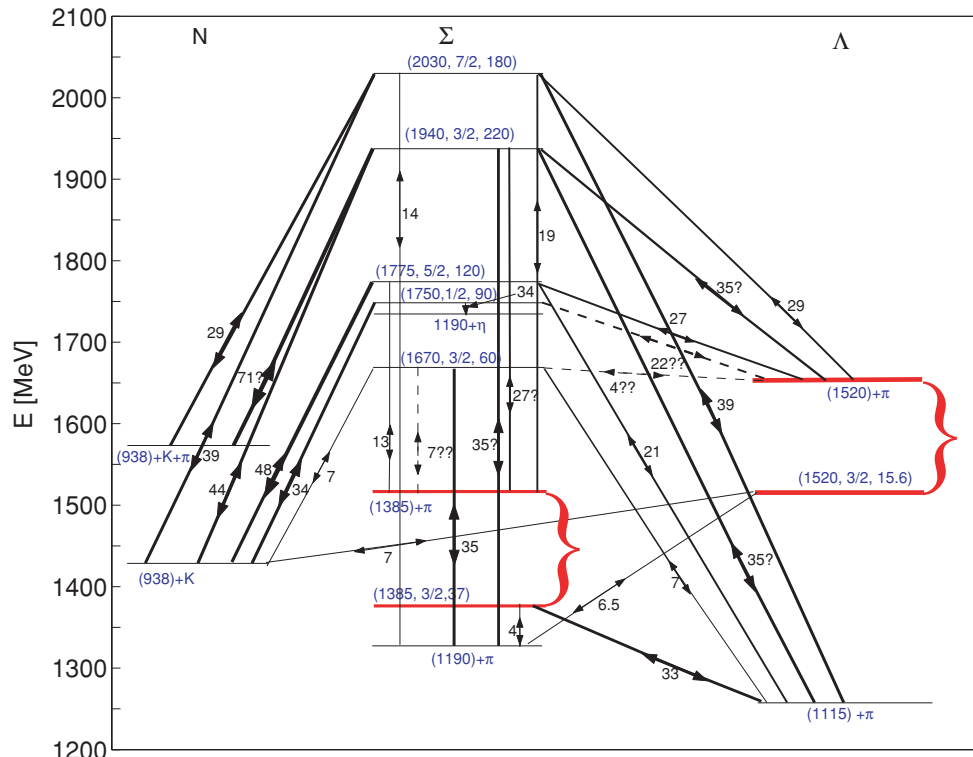
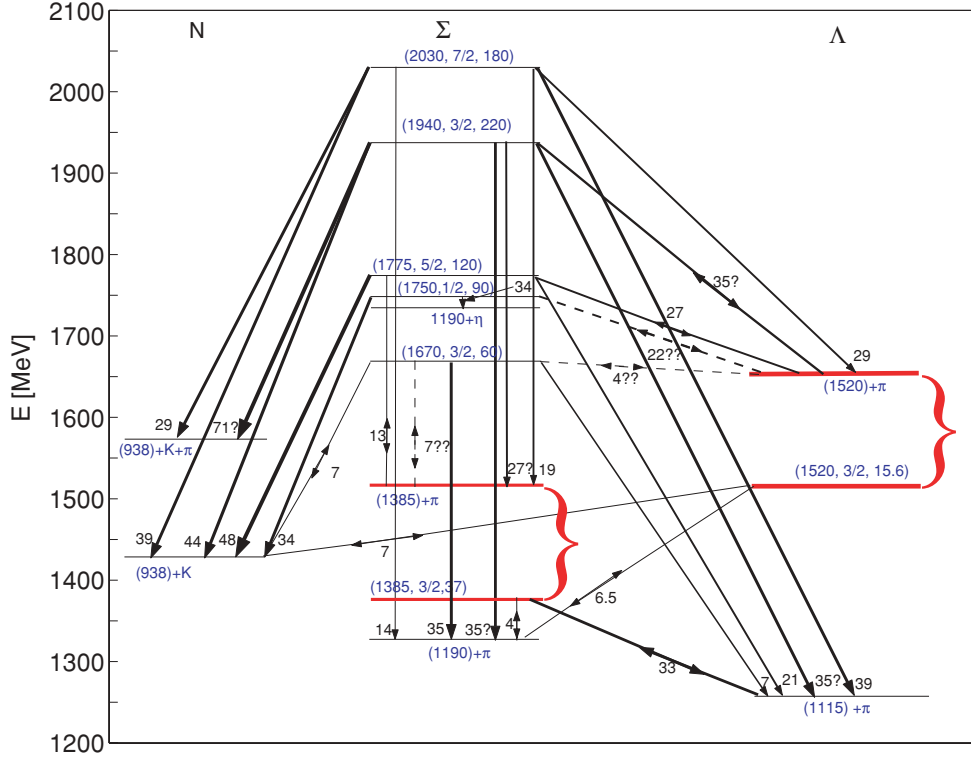


FIG. 1. (Color online) Reactions scheme for  $\Lambda(1520)$  and  $\Sigma(1385)$  population evolutions.


 FIG. 2. (Color online) Reactions scheme for  $\Lambda(1520)$  and  $\Sigma(1385)$  interactions in the “dead channel” model.

Hereto we note that (several)  $\Sigma^*$  involved in Eq. (4) participate in further reactions:

$$\Lambda(1115) + \pi \leftrightarrow \Sigma^*; \quad (5)$$

$$\Sigma(1190) + \pi \leftrightarrow \Sigma^*; \quad (6)$$

$$N + K \leftrightarrow \Sigma^*; \quad (7)$$

$$\Sigma(1385) + \pi \leftrightarrow \Sigma^*; \quad (8)$$

$$\Delta + K \leftrightarrow \Sigma(1940, 2030); \quad (9)$$

$$N + K(892) \leftrightarrow \Sigma(1940); \quad (10)$$

$$\Sigma + \eta \leftrightarrow \Sigma(1750). \quad (11)$$

All reactions shown above can excite  $\Sigma^*$  resonances. Since the mass of  $\Lambda(1520)$  is near to the  $\Sigma^*$  mass, the yield of  $\Lambda(1520)$  is effectively depleted by the reaction chain

$$\Lambda(1520) + \pi \rightarrow \Sigma^* \rightarrow N + K, \text{ etc.} \quad (12)$$

The balancing two step back-reaction can also occur, especially once  $\Lambda(1520)$  has been depopulated. Thus a dynamical reduced detailed balance yield of  $\Lambda(1520)$  would result if the system were at fixed volume rather than expanding.

The multiplicity of  $\Sigma(1385)$  is mostly determined by its dominant decay and production in the reaction

$$\Lambda(1115) + \pi \leftrightarrow \Sigma(1385), \quad (13)$$

and to a lesser extent by the reaction

$$\Sigma(1190) + \pi \leftrightarrow \Sigma(1385). \quad (14)$$

The resonance  $\Sigma(1385)$  participates further in reactions with heavier  $\Sigma^*$ ; see reaction (8), but strength of these interactions is smaller than for similar reactions with  $\Lambda(1520)$  and smaller

than the decay width of  $\Sigma(1385)$ . Thus we find that the influence of these reactions on  $\Sigma(1385)$  yield is small. Another reason for a reduced effective depletion rate of  $\Sigma(1385)$  is that a lesser fraction of this resonance is needed to excite  $\Sigma^*$ . Thus in such a reaction the depopulation effect decreases because of a larger mass difference between  $\Sigma(1385)$  and  $\Sigma^*$  in comparison with  $\Lambda(1520)$  and  $\Sigma^*$ .

The reactions scheme for  $\Lambda(1520)$  reactions with dead channels is shown in Fig. 2. The difference between Figs. 1 and 2 is that some of the reaction lines have single-directional arrows, as is stipulated by the condition Eq. (2).

### B. Resonances densities, time evolution equations

The evolution in time of the resonance yield is described by a master equation, where the process of resonance formation in scattering is balanced by the natural resonance decay:

$$\frac{1}{V} \frac{dN_3}{dt} = \sum_i \frac{dW_{1+2 \rightarrow 3}^i}{dV dt} - \sum_j \frac{dW_{3 \rightarrow 1+2}^j}{dV dt}, \quad (15)$$

where subscripts  $i, j$  denote different reactions channels when available. We further allow different subscripts  $i, j$  for the case where there are dead channels. Thus  $dW_{1+2 \rightarrow 3}^i/dV dt$  and  $dW_{3 \rightarrow 1+2}^j/dV dt$  are invariant rates (per unit volume and time) for particle 3 production and decay, respectively. In case all reactions occur in both directions the total number of fusion channels is the same as the total number of decay channels.

Allowing for Fermi-blocking and Bose enhancement in the final state, where by designation particles 1 and 3 are fermions

(heavy baryons) and particle 2 is a boson (often light pion) we have for the two rates

$$\begin{aligned} \frac{dW_{3 \rightarrow 1+2}^j}{dV dt} &= \int \frac{g_3 d^3 p_3}{2E_3(2\pi)^3} f_3 \int \frac{d^3 p_1}{2E_1(2\pi)^3} (1 - f_1) \\ &\times \int \frac{d^3 p_2}{2E_2(2\pi)^3} (1 + f_2) (2\pi)^4 \delta^4 \\ &\times (p_1 + p_2 - p_3) \\ &\times \frac{1}{g_3} \sum_{\text{spin}} |\langle p_3 | M^j | p_1 p_2 \rangle|^2, \end{aligned} \quad (16)$$

$$\begin{aligned} \frac{dW_{1+2 \rightarrow 3}^i}{dV dt} &= \int \frac{g_1 d^3 p_1}{2E_1(2\pi)^3} f_1 \int \frac{g_2 d^3 p_2}{2E_2(2\pi)^3} f_2 \\ &\times \int \frac{d^3 p_3}{2E_3(2\pi)^3} (1 - f_3) (2\pi)^4 \delta^4 \\ &\times (p_1 + p_2 - p_3) \\ &\times \frac{1}{g_1 g_2} \sum_{\text{spin}} |\langle p_1 p_2 | M^i | p_3 \rangle|^2, \end{aligned} \quad (17)$$

where  $g_i$ ,  $i = 1, 2, 3$  is particles degeneracy. The Bose distribution function for particle 2 is

$$f_2 = \frac{1}{\Upsilon_2^{-1} e^{u \cdot p_2/T} - 1}, \quad (18)$$

and Fermi for particles 1,3 are

$$f_j = \frac{1}{\Upsilon_j^{-1} e^{u \cdot p_j/T} + 1}, \quad j = 1, 3. \quad (19)$$

Here  $\Upsilon_i$  is particles fugacity, and  $u \cdot p_i = E_i$ , for  $u^\mu = (1, \vec{0})$  in the rest frame of the heat bath where  $d^4 p \delta_0(p_i^2 - m_i^2) \rightarrow d^3 p_i/E_i$  for each particle. Hence, Eqs. (16) and (17) are Lorentz invariant, and thus as presented these rates can be evaluated in any convenient frame of reference. Normally, this is the frame co-moving with the thermal volume element.

For the heavy baryon (resonances), particles 2,3, we can work using the expansion of the relativistic distribution, the first term is the Boltzmann limit:

$$\frac{N_i}{V} = \Upsilon_i \frac{T^3}{2\pi^2} g_i x_i^2 K_2(x_i), \quad (20)$$

where  $x_i = m_i/T$ ,  $K_2(x)$  is the Bessel function (not to be mixed up with particle 2). However, we use the complete Bose distribution to describe pions.

We introduce in medium lifespan of particle 3:

$$\frac{1}{\tau_3} \equiv \frac{\sum_i R_{123}^i}{V^{-1} dN_3/d\Upsilon_3}, \quad (21)$$

and, similarly, channel lifespan  $\tau_3^i$ , omitting the sum  $\sum_i$ . Here the rate  $R_{123}$  is

$$\begin{aligned} R_{123}^i &= \iiint \frac{d^3 p_1 d^3 p_2 d^3 p_3}{8E_1 E_2 E_3 (2\pi)^5} f_1 \Upsilon_1^{-1} f_2 \Upsilon_2^{-1} f_3 \Upsilon_3^{-1} \\ &\times \delta^4(p_1 + p_2 - p_3) e^{u \cdot p_3/T} \sum_{\text{spin}} |\langle p_1 p_2 | M^i | p_3 \rangle|^2. \end{aligned} \quad (22)$$

$R$  is independent of the fugacity in the Boltzmann-limit. In Sec. II C we will see in what way the in-medium decay rate

varies from the free space decay rate. This is due to the effect of quantum enhancement, and the fact that a particle emerged in a thermal bath with a finite temperature. A particle is not decaying in its rest frame.

The production and decay rates are connected to each other by the detailed balance relation [11,12]:

$$\Upsilon_1^{-1} \Upsilon_2^{-1} \frac{dW_{1+2 \rightarrow 3}}{dV dt} = \Upsilon_3^{-1} \frac{dW_{3 \rightarrow 1+2}}{dV dt} = R_{123}. \quad (23)$$

Using detailed balance Eq. (23) we obtain for fugacity  $\Upsilon_3$  the evolution equation [11,12]:

$$\frac{d\Upsilon_3}{d\tau} = \sum_i \Upsilon_1^i \Upsilon_2^i \frac{1}{\tau_3^i} + \Upsilon_3 \left( \frac{1}{\tau_T} + \frac{1}{\tau_S} - \sum_j \frac{1}{\tau_3^j} \right), \quad (24)$$

where we have also introduced characteristic time constants of temperature  $T$  and entropy  $S$  evolution

$$\frac{1}{\tau_T} = -\frac{d \ln(x_3^2 K_2(x_3))}{dT} \dot{T}, \quad (25)$$

$$\frac{1}{\tau_S} = -\frac{d \ln(VT^3)}{dT} \dot{T}. \quad (26)$$

The entropy term is negligible,  $\tau_S \gg \tau_3, \tau_T$  since we implement near conservation of entropy. We implement this in the way which would be exact for massless particles taking  $VT^3 = \text{Const}$ . Thus there is some entropy growth in HG evolution to consider, but it is not significant. In order to evaluate the magnitude of  $\tau_T$  we use the relation between Bessel functions of order 1 and 2 (not to be mixed up with particles 1,2)  $d(z^2 K_2(z))/dz = -z^2 K_1(z)$ . We obtain

$$\frac{1}{\tau_T} = -\frac{K_1(x_3)}{K_2(x_3)} x_3 \frac{\dot{T}}{T}, \quad (27)$$

$\tau_T > 0$ . We invoke a model of matter expansion of the type used, e.g., in [15], where the longitudinal and transverse expansion is considered to be (nearly) independent. In this model we have

$$\frac{\dot{T}}{T} = -\frac{1}{3} \left( \frac{2(v\tau/R_\perp) + 1}{\tau} \right), \quad (28)$$

where  $R_\perp$  is the transverse radius,  $v$  is the velocity of expansion in the transverse dimension. All flow parameters (or temperature dependence on  $\tau$ ) are the same as in [9]. For a static system with  $\tau_T \rightarrow 0$  we see that Eq. (24) has transient stable population points whenever

$$\sum_i \Upsilon_1^i \Upsilon_2^i \frac{1}{\tau_3^i} - \Upsilon_3 \sum_j \frac{1}{\tau_3^j} = 0. \quad (29)$$

Next we address the functional dependence on time of  $\Upsilon_1, \Upsilon_2$ . In the equation for  $\Upsilon_1$  we have terms which compensate what is lost/gained in  $\Upsilon_3$  see Eq. (24). Further we have to allow that particle '1' itself plays the role of particle 3 (for example this is clearly the case for  $\Lambda(1520)$ ). That allows a chain of populations relations as follows:

$$(1' + 2' \leftrightarrow 1) + 2 \leftrightarrow 3. \quad (30)$$

Then we obtain

$$\begin{aligned} \frac{d\Upsilon_1}{d\tau} = & \Upsilon_3 \sum_k \frac{1}{\tau_3^k} \frac{dN_3^k/d\Upsilon_3^k}{dN_1/d\Upsilon_1} - \sum_n \Upsilon_1 \Upsilon_2^n \frac{1}{\tau_3^n} \frac{dN_3^n/d\Upsilon_3^n}{dN_1/d\Upsilon_1} \\ & + \Upsilon_1 \left( \frac{1}{\tau_T} + \frac{1}{\tau_S} - \sum_j \frac{1}{\tau_j^i} \right) + \sum_i \Upsilon_1^i \Upsilon_2^i \frac{1}{\tau_1^i}. \end{aligned} \quad (31)$$

The ratios of derivative of  $N_i$  seen in the first line are due to the definition of relaxation time Eq. (21). The system of equations for baryons closes with the equation for  $\Upsilon_1$

$$\begin{aligned} \frac{d\Upsilon_{1'}}{d\tau} = & \Upsilon_1 \sum_k \frac{1}{\tau_1^k} \frac{dN_1^k/d\Upsilon_1^k}{dN_{1'}/d\Upsilon_{1'}} - \sum_n \Upsilon_{1'} \Upsilon_2^n \frac{1}{\tau_1^n} \frac{dN_1^n/d\Upsilon_1^n}{dN_{1'}/d\Upsilon_{1'}} \\ & + \Upsilon_{1'} \left( \frac{1}{\tau_T} + \frac{1}{\tau_S} \right). \end{aligned} \quad (32)$$

In the present setting  $\Upsilon_{2=\pi} = \text{Const.}$  by virtue of entropy conservation (see discussion below) and the same applies to the case  $2' = \pi$ . However, if either particle 2 or  $2'$  is a kaon, we need to follow the equation for  $\Upsilon_{2,2'=K}$  which is analogous to equation for particle 1 or  $1'$ .

The evolution equations can be integrated once we determine the *initial* values of particle densities (fugacities) established at hadronization/chemical freeze-out. We determine these for RHIC head-on Au-Au collisions at  $\sqrt{s_{NN}} = 200$  GeV. We introduce the initial hadron yields inspired by a picture of a rapid hadronization of QGP in which quarks combine into final state hadrons. For simplicity we assume here that the net baryon yield at central rapidity is negligible. Thus the baryon-chemical and strangeness potentials vanish. The initial yields of mesons ( $q\bar{q}$ ,  $s\bar{q}$ ) and baryons ( $qqq$ ,  $qq\bar{s}$ ) are controlled aside of the ambient temperature  $T$  by the constituent light quark fugacity  $\gamma_q$  and the strange quark fugacity  $\gamma_s$ .

The strangeness pair-yield in QGP is maintained in transition to HG. This fixes the initial value of  $\gamma_s$ . In fact, since we investigate here relative chemical equilibrium reactions our results do not depend significantly on the exact initial value  $\gamma_s$  and/or strangeness content. The entropy conservation at hadronization fixes  $\gamma_q$ . For hadronization temperature  $T(t=0) \equiv T_0 = 180$  MeV,  $\gamma_q = 1$ . However, when  $T_0 < 180$  MeV,  $\gamma_q > 1$  in order to have entropy conserved at chemical freeze-out. At  $T_0 = 140$  MeV  $\gamma_q = 1.6$  that is close to maximum possible value of  $\gamma_q$ , defined by Bose-Einstein condensation condition [10].

For reactions, such as shown in Eq. (1), we have (lower index defines particle considered, where  $Y \equiv \Sigma, \Lambda$  is a hyperon)

$$\Upsilon_{(1=Y)}^0 = \gamma_q^2 \gamma_s, \quad \Upsilon_{(2=\pi)}^0 = \gamma_q^2; \quad (33)$$

or

$$\Upsilon_{(1=N)}^0 = \gamma_q^3, \quad \Upsilon_{(2=K)}^0 = \gamma_q \gamma_s; \quad (34)$$

where the particle 1 in reaction (1) is a baryon and particle 2 is a meson. The particle 3 is always a strange baryon:

$$\Upsilon_{(3=Y)}^0 = \gamma_q^2 \gamma_s. \quad (35)$$

Note that for  $\gamma_q > 1$  we have always initially

$$\left. \frac{\Upsilon_1 \Upsilon_2}{\Upsilon_3} \right|_{t=0} = \gamma_q^2 \geq 1. \quad (36)$$

As a consequence initially the pair of particles 1,2 reacts into 3.

As already noted, we do not need to follow the evolution in time for the pion yield, which is fixed by conservation of entropy per unit rapidity, as incorporated in Eq. (28). Thus it is (approximately) a constant of motion. This can be seen recalling that the entropy per pion is nearly 4 within the domain of temperatures considered. Thus the conservation of entropy implies that pion number is conserved. With  $VT^3 \simeq \text{Const.}$ , this further implies that during the expansion

$$\Upsilon_\pi = \gamma_q^2 = \text{Const.},$$

which we keep at the initial value.

### C. In medium lifespan calculations

In our calculations we take into account the influence of the medium on resonance lifespan and the effect of the motion of the decaying particle with respect to the thermal rest frame. In [11,12] it was noted that the decay rate  $R_{123}$ , Eq. (22), of particle 3 (density) in a thermally equilibrated system can be cast into a form which involves the free space decay rate:

$$R_{123} = \frac{m_3}{\tau_0} \int_0^\infty \frac{p_3^2 dp_3}{E_3} \frac{\Upsilon_3^{-1} e^{E_3/T}}{\Upsilon_3^{-1} e^{E_3/T} \pm 1} \Phi(p_3), \quad (37)$$

where function  $\Phi(p_3)$  for reaction (13)  $\Sigma(1385) \leftrightarrow \Lambda + \pi$  is

$$\Phi(p_3) = \frac{1}{b(e^{E_3/T} + \Upsilon_\pi \Upsilon_\Lambda)} \ln \frac{(\Upsilon_\Lambda e^b + e^{-a_2})(e^{a_1} - \Upsilon_\pi e^{-b})}{(\Upsilon_\Lambda e^{-b} + e^{-a_2})(e^{a_1} - \Upsilon_\pi e^b)}. \quad (38)$$

$$a_1 = \frac{E_1^* E_3}{m_3 T}, \quad a_2 = \frac{E_2^* E_3}{m_3 T}, \quad b = \frac{p^* p_3}{m_3 T}.$$

Here  $p^* = p_1 = p_2$  and  $E_{1,2}^* = \sqrt{p^{*2} + m_{1,2}^2}$  are the magnitude of the momentum and, respectively, the energy, of particles 1 and 2 in the rest frame of the particle 3. From energy conservation:

$$E_{1,2}^* = \frac{m_3^2 \pm (m_1^2 - m_2^2)}{2m_3}, \quad (39)$$

$$p^{*2} = E_{1,2}^2 - m_{1,2}^2 = \frac{m_3^2}{4} - \frac{m_1^2 + m_2^2}{2} + \frac{(m_1^2 - m_2^2)^2}{4m_3^2}.$$

Here fugacities for  $\Lambda$  and  $\pi$  correspond to those for particles 1 and 2, respectively. For the temperatures of interest (hadronization of QGP and below)  $m_\Lambda$  and  $m_\Sigma \gg T$ . With sufficient accuracy we can write

$$\Phi(p_3) \simeq \frac{1}{b e^{E_3/T}} \ln \frac{(e^{a_1+b} - \Upsilon_\pi)}{(e^{a_1-b} - \Upsilon_\pi)}. \quad (40)$$

There are no significant medium effects upon decay rate of  $\Sigma(1385)$  and  $\Lambda$  resonances. However the pions have energy  $E_2^* = 250$  MeV [Eq. (39)] in the  $\Sigma$  rest frame and the Bose

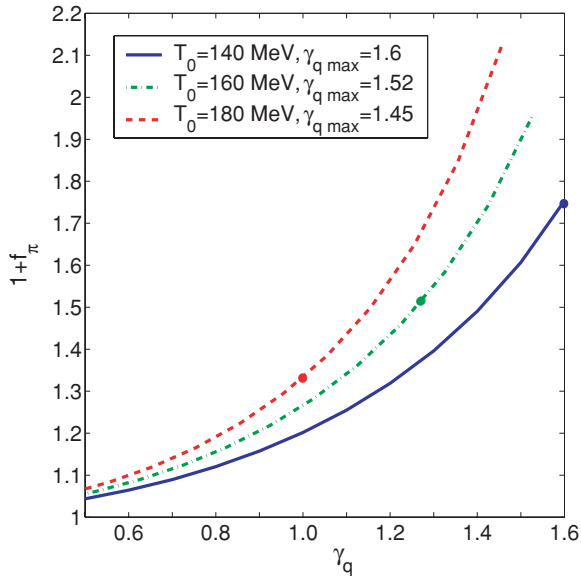


FIG. 3. (Color online) The Bose enhancement factor  $1 + f_\pi(E_1^*)$  in  $\Sigma(1385)$  rest frame as a function of light quark fugacity  $\gamma_q$  for the reaction  $\Sigma(1385) \leftrightarrow \Lambda\pi$  at  $T = 140$  MeV (blue, solid line), at 160 MeV (green, dash-dot line) and 180 MeV (red, dashed line). The dots show the initial value of fugacities for the three possible hadronization cases.

enhancement effect is possible in the oversaturated hadronic gas after QGP hadronization.

For the low temperatures considered here we can assume that  $\Sigma$  resonances almost do not move. Thus the enhancement effect in the thermal bath frame is close to the enhancement in the  $\Sigma(1385)$  rest frame. The decay rate increases by Bose enhancement factor  $1 + f_\pi$  (here  $f_\pi = f_\pi(E_2^*, T)$ ). In Fig. 3 we show Bose enhancement factor as a function of light quark fugacity  $\gamma_q$  for temperature  $T_0 = 140$  MeV (blue, solid line),  $T_0 = 160$  MeV (green, dash-dot line),  $T_0 = 180$  MeV (red, dashed line). The large dots show Bose enhancement factor for our initial  $\gamma_q$  determined from entropy conservation in fast hadronization. The fugacity  $\gamma_q = 1.6$  is close to maximum expected value at  $T_0 = 140$  MeV. The maximum fugacities for each temperature correspond to Bose-Einstein singularity. The Bose enhancement effect is largest for maximum  $\gamma_q$  and it diminishes for small  $\gamma_q$ . At fixed entropy the greatest enhancement is for smallest ambient temperature, see the dot on solid line in Fig. 3.

In Fig. 4 we show the corresponding decrease in the lifespan, the ratio  $\tau_3/\tau_0$  as a function of temperature  $T$  in the reaction  $\Sigma(1385) \leftrightarrow \Lambda\pi$ . We consider temperature range from corresponding hadronization temperature until  $T = 70$  MeV. We assumed, that  $\Upsilon_\pi$  is a constant. Fugacities of heavy resonances do not influence the result. The lowest  $\tau_3/\tau_0$  ratio is for  $\gamma_q = 1.6$  at  $T_0 = 140$  MeV when we have maximum value of  $\gamma_q$  for given temperature. If we compare this value of  $\tau_3/\tau_0 = 0.65$  with inverse Bose enhancement factor  $1/(1 + f_\pi(E_2^*, T)) = 0.54$  for this  $T$  and  $\gamma_q$  (see Fig. 3) we see that these values are near to each other (difference is about 20%) as expected for  $m_\Sigma \gg T$ . For smaller  $T$ ,  $\gamma_q$  decay time goes to its vacuum value.

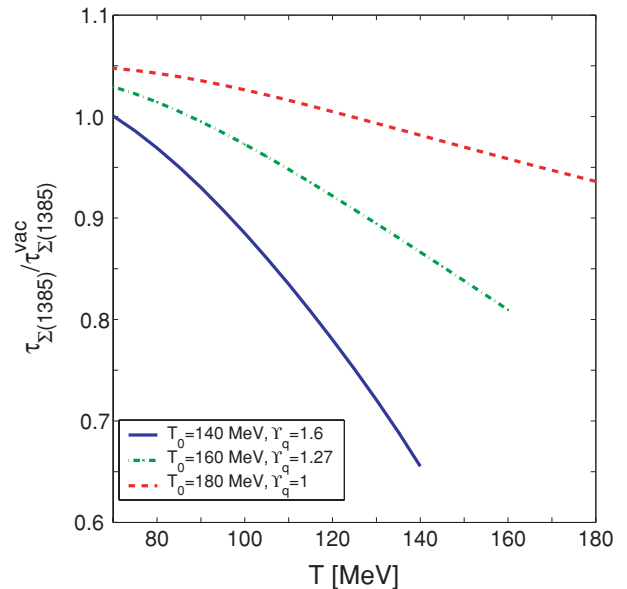


FIG. 4. (Color online) The ratio of the in medium lifespan  $\tau_3$  with the vacuum lifespan  $\tau_0$  as a function of temperature  $T$  for the reaction  $\Sigma(1385) \leftrightarrow \Lambda\pi$ . The dashed (red) line is for hadronization at  $T_0 = 180$  MeV,  $\gamma_q = 1.0$ ; the dot-dashed line (green) for hadronization at 160 MeV,  $\gamma_q = 1.27$ ; solid line (blue) is for hadronization at 140 MeV and  $\gamma_q = 1.6$ .

The same calculations are applicable for heavier  $\Sigma^*$ . When the difference of mass of the initial and final state resonance decreases, the Bose enhancement effect increases, since it involves small momenta. The largest effect is for reaction  $\Sigma(1670) \leftrightarrow \Lambda(1520) + \pi$ . On the other hand, for the reactions which satisfy condition (2) the enhancement effect becomes so small that we do not need to include it in our calculations.

### III. NUMERICAL RESULTS

#### A. Evolution of fugacities

In order to evaluate the  $\Lambda(1520)$  and  $\Sigma(1385)$  multiplicities we must integrate Eq. (24), or Eq. (31), or Eq. (32) for each particle involved in Fig. 1, and perform similar operations for reactions with dead channels in Fig. 2. This system of equations includes equations for  $\Lambda(1520)$ ,  $\Sigma(1385)$ , five equations for  $\Sigma^*$ s, equations for  $K(892)$  and  $\Delta$  and equations for ground states  $\Lambda(1115)$ ,  $\Sigma(1190)$ ,  $N$ ,  $K$ . All reactions in Fig. 1 are included. We solve this system of equations numerically, using classical fourth order Runge-Kutta method.

Particle fugacities, except  $\Upsilon_\pi$ , change rather rapidly. Figure 5 shows the computed  $\Upsilon(t)$  as a function of temperature  $T(t)$ . We present here the scenario in which all reactions evolve in both directions, for the initial condition  $\gamma_s = \gamma_q$ . The time, corresponding to the temperature shown at the bottom, is shown at the top of Fig. 5, in each frame. On the left we have hadronization at 140 MeV, in the middle at 160, and to the right at 180 MeV. Each frame has the same scale size for temperature unit, not time. For  $\Upsilon_{\Sigma^*}$  we show two possible evolution examples, for  $\Sigma_{1750}$  (dash-dot dark line) and  $\Sigma(1775)$  (dashed line). These resonances have

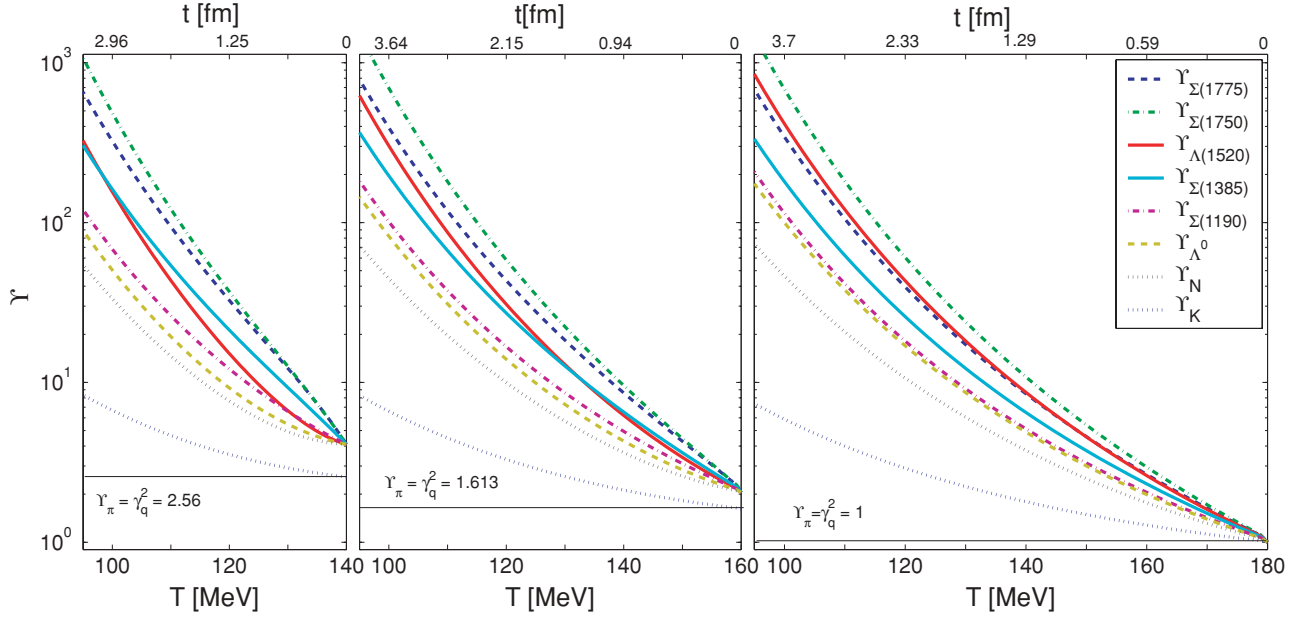


FIG. 5. (Color online) The fugacities  $\Upsilon$  for selected particles are shown as a function of temperature  $T(t)$ , for  $T_0 = 140$  MeV on the left, for  $T_0 = 160$  MeV in the middle, and for  $T_0 = 180$  MeV, on the right. See text for further details.

significant influence on the  $\Lambda(1520)$  yield. The solid lines are for  $\Upsilon_{\Lambda(1520)}$  (upper, red line) and  $\Upsilon_{\Sigma(1385)}$  (lower, light blue line). The dash-dot and dashed light lines are for  $\Upsilon_{\Sigma(1190)}$  and  $\Upsilon_{\Lambda^0}$ , respectively. The upper dotted line is for  $\Upsilon_N$  and lower dotted line is for  $\Upsilon_K$ .

An important feature is that the  $\Upsilon$ s of massive hadron (resonances) increase very fast when  $T$  decreases. This is so since in absence of a rapid reequilibration reactions, multiplicity of given resonance must be conserved. Then, according to Eq. (20)  $\Upsilon_i \propto 1/K_2(m_i/T)$ , and thus for large  $m_i$   $\Upsilon_i \propto \exp(m_i/T)$ . We would expect  $\Upsilon_i > \Upsilon_j$ , when  $m_i > m_j$ , and  $T$  decreases. This behavior is just like we found for the case of large charm fugacity [10]. However, because of the decay and regeneration reactions there are some deviations from this expectation in Fig. 5.

For  $T_0 = 180$  MeV in most cases  $\Upsilon_3 > \Upsilon_1 \Upsilon_2$  ( $t > 0$ ). Massive resonances decay to lower mass particles. The result is defined by resonance mass, its decay width and decay products. For example  $\Upsilon_{\Sigma(1775)}$  is smaller than  $\Upsilon_{\Sigma(1750)}$  and  $\Upsilon_{\Lambda(1520)}$ , because of its large decay width. Therefore excitation of  $\Sigma(1775)$  by  $\Lambda$  slightly dominates over  $\Sigma(1775)$  decay to  $\Lambda(1520)$  even in this case, when for most resonances the decay is dominant. For smaller initial hadronization temperatures  $\Upsilon_{\Lambda(1520)}$  becomes smaller than  $\Upsilon_{\Sigma(1775)}$ , and even smaller than  $\Upsilon_{\Sigma(1385)}$  in some range of temperatures. This suppression occurs because of  $\Sigma(1775)$ , and others  $\Sigma^*$  regeneration. Because of large  $\Upsilon_\pi$ ,  $\Upsilon_{\Sigma(1775)} < \Upsilon_{\Lambda(1520)} \Upsilon_\pi$ , the  $\Sigma(1775)$  production by  $\Lambda(1520)$  is dominant in the full range of  $T$  considered here.

### B. Final $\Lambda(1520)$ and $\Sigma(1385)$ multiplicities

In this section we consider the evolution of the multiplicity of resonances  $\Lambda(1520)$ ,  $\Sigma(1385)$ ,  $\Sigma(1775)$  during the kinetic

phase. We use the Boltzmann yield limit, Eq. (20). By the symbol  $X(T)$  we refer to a particular resonance, and  $X_0$  is the initial multiplicity for that resonance. The dynamic yield of this resonance may be expressed as

$$\frac{X(T)}{X_0} = \frac{\Upsilon_X(t) T(t)^3 K_2(m_X/T(t))}{\Upsilon_{X_0} T_0^3 K_2(m_X/T_0)}. \quad (41)$$

Figure 6 shows this yield as a function of  $T(t)$  for  $X = \Sigma(1385)$  (left) and  $X = \Lambda(1520)$  (right). We consider three initial conditions, temperature  $T_0 = 140, 160, 180$  MeV, with corresponding  $\gamma_q = 1.6, 1.27, 1.0$ , respectively. The solid lines correspond for the model with dead channels and dashed one are for case when all reactions are symmetric in both directions. The thin dotted vertical line at  $T = 120$  MeV marks the kinetic freeze-out temperature, assumed before in [9]. The main result is that the resulting relative yields for  $\Lambda(1520)$  and  $\Sigma(1385)$  behave qualitatively different from each other. In particular, as the temperature decreases, for the case  $T_0 = 140$  MeV we observe a strong yield suppression for  $\Lambda(1520)$ , and a strong enhancement for  $\Sigma(1385)$  (as compared to initial SHM yields).

To better understand the mechanism of  $\Lambda(1520)$  suppression, we analyze in some detail the case of  $\Sigma(1775)$  and  $\Sigma(1750)$  decay and production rates  $dW/dVdt$ . We assume here that these reactions can go in both directions. In Fig. 7 we show the reactions rates for the principal channels of decay and production as a functions of temperature  $T$  for  $\Sigma(1775)$  (left) and  $\Sigma(1750)$  (right), for the case of initial temperature  $T_0 = 140$  MeV which provides the largest  $\Lambda(1520)$  suppression. Solid lines are for the reaction  $\Sigma \leftrightarrow \Lambda(1520) + \pi$ , dash-dot lines are for reaction  $\Sigma \leftrightarrow N + K$ , dashed lines are for reaction  $\Sigma \leftrightarrow \Lambda^0 + \pi$ . Two sets of lines are presented for the decay (on-line blue) and backward fusion reaction (on-line red), respectively.

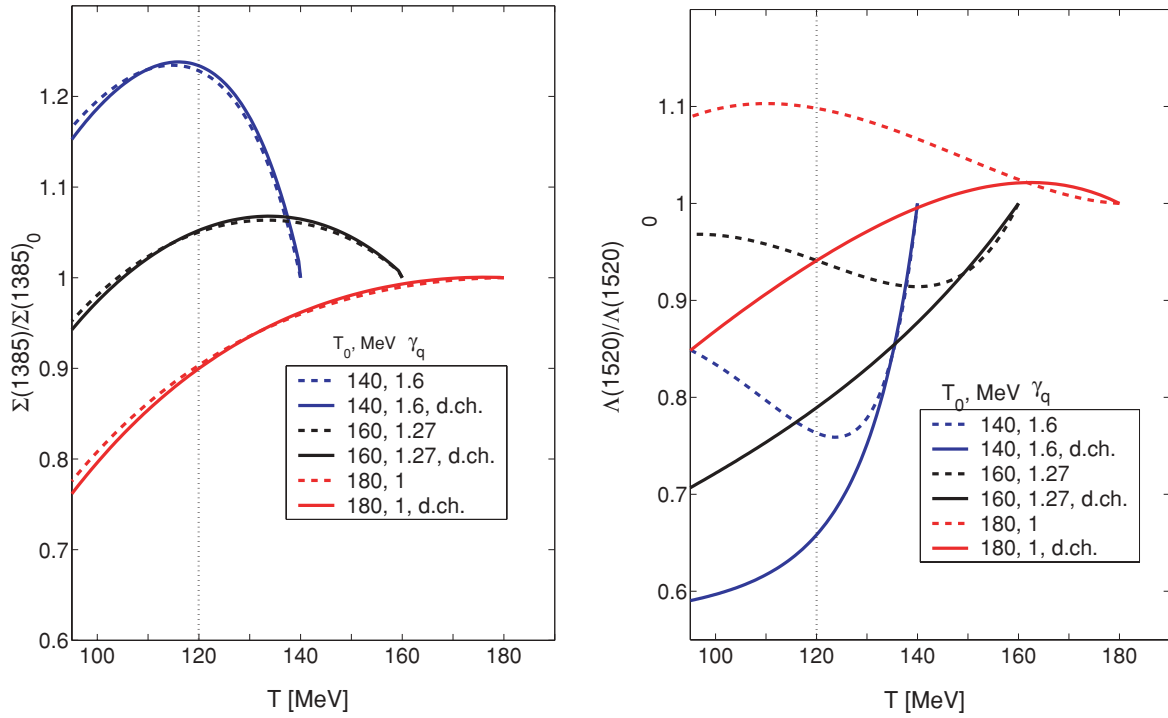


FIG. 6. (Color online) The ratio  $\Sigma(1385)/\Sigma(1385)_0$  on left and  $\Lambda(1520)/\Lambda(1520)_0$  on right as a functions of temperature  $T(t)$  for different initial hadronization temperatures  $T_0 = 140, 160,$  and  $180$  MeV (blue/bottom, black/middle, and red/top lines, respectively). Solid lines are for calculations with dead channels, dashed lines are for calculations without dead channels.

As temperature decreases, all rates  $dW/dtdV$  are increasing rapidly. This is mainly because fugacities  $\Upsilon$  increase nearly exponentially when number of particles is conserved, see Fig. 5. We see that at the beginning of the kinetic phase all reactions go in the direction of  $\Sigma(1775)$  production,

since  $\Sigma(1775)$  production rate is larger than its decay rate for all channels. Then at first  $\Sigma(1775) \leftrightarrow \Lambda^0 + \pi$  decay rate becomes dominant over  $\Sigma(1775)$  production rate in this channel, followed by the same for  $\Sigma(1775) \leftrightarrow N + K$  channel.

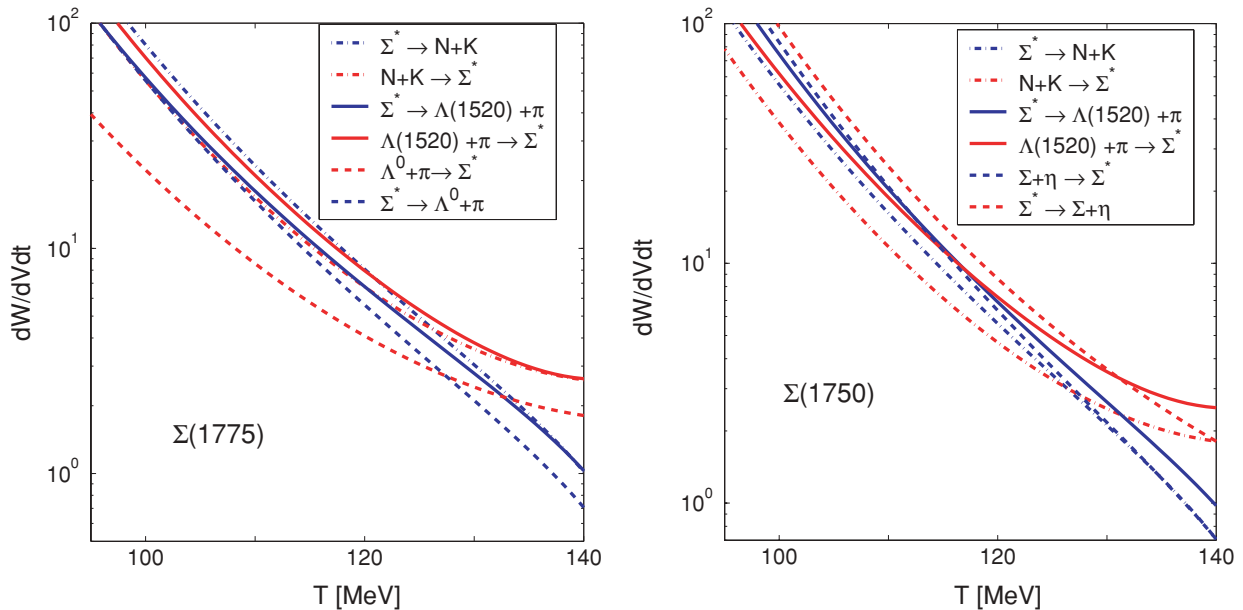


FIG. 7. (Color online) The rates for main channels of  $\Sigma(1775)$  (on the left) and  $\Sigma(1750)$  (on the right) decay and production as a functions of temperature  $T$  in the case when all reactions go in both directions and  $T_0 = 140$  MeV. Solid lines are for reaction  $\Sigma^* \leftrightarrow \Lambda(1520) + \pi$ ; dash-dot lines are for reaction  $\Sigma^* \leftrightarrow N + K$ ; dashed lines are for reaction  $\Sigma(1775) \leftrightarrow \Lambda^0 + \pi$  on the left and  $\Sigma(1750) \leftrightarrow \Sigma + \eta$  on the right; blue and red lines are for decay and backward fusion reaction, respectively.

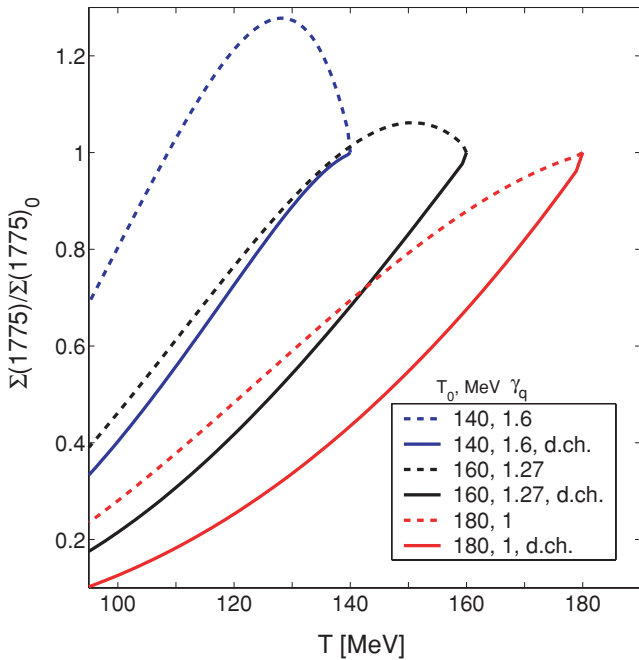


FIG. 8. (Color online) The ratio  $\Sigma(1775)/\Sigma(1775)_0$  as a functions of temperature  $T(t)$  for different initial hadronization temperatures  $T_0 = 140, 160,$  and  $180$  MeV (blue/bottom, black/middle, and red/top lines), respectively. Solid lines are for calculations with dead channels, dashed lines are for calculations without dead channels.

For the reaction  $\Sigma(1775) \leftrightarrow \Lambda(1520) + \pi$  backward reaction is always dominant. As result, during the kinetic phase always more  $\Lambda(1520)$  resonances are excited into  $\Sigma(1775)$  than they are produced by  $\Sigma(1775)$  decay. The reason for this is the decay of  $\Sigma(1775)$  to the other channels, as long as  $\Upsilon_{\Sigma(1775)} < \Upsilon_{\Lambda(1520)} \Upsilon_{\pi}$ . The lighter is the total mass of decay products, the earlier the decay reaction becomes dominant. This is due to the fact that the fugacity of  $\Upsilon$  for heavier particles increases faster with expansion. Therefore, the decay rate becomes dominant earlier, when the difference between initial and final mass is larger. The net result is  $\Lambda(1520)$  suppression by  $\Sigma(1775)$  excitation.

In Fig. 8 we show the yield of  $\Sigma(1775)$  normalized by its initial yield at hadronization:  $\Sigma(1775)/\Sigma(1775)_0$  as a function of  $T(t)$ . Like in the other figures above, solid lines are for the dead channels and dashed lines are for case when reactions go in both directions, solid (blue) lines are for  $T_0 = 140$  MeV, solid (black) lines for  $T_0 = 160$  MeV, and solid (red) lines are for  $T_0 = 180$  MeV. Each of the lines can be identified by their initial  $T$ -value. We see that when all reactions go in both direction the ratio  $\Sigma(1775)/\Sigma(1775)_0$  increases at first similar to  $\Sigma(1385)/\Sigma(1385)_0$  and  $\Delta(1230)/\Delta(1230)_0$  ratios [9].

Compared to these ratios,  $\Sigma(1775)/\Sigma(1775)_0$  ratio reaches its maximum value earlier, and after the maximum, the yield of  $\Sigma(1775)$  decreases faster. The reason for this behavior is that the mass of  $\Sigma(1775)$  is larger. The phase space occupancy  $\Upsilon_{\Sigma(1775)}$ , and therefore its decay rates, increase faster than the fugacity and decay rates for  $\Sigma(1385)$  and  $\Delta(1230)$ . Therefore

decays  $\Sigma(1775)$  to some channels and its total decay rate become dominant earlier (see Fig. 7). Although the total decay width of  $\Sigma(1775)$  is approximately the same as for  $\Delta(1230)$ , the maximum value of this ratio is smaller.

Said differently, the maximum yield of  $\Sigma(1775)$  does not have time to reach the value as high as that for  $\Delta(1230)$ . We thus learn that the time evolution of the yield of resonances with large decay width depends not only on their decay width, but also on mass difference between initial and final states. Similar time evolution occurs for the other  $\Sigma^*$ , which quantitatively depends on their mass, decay products masses and decay width.

For most  $\Sigma^*$ s, the decay products in the channel  $\Lambda(1520) + \pi$  are heavier than the decay products in others channels, which are thus favored by phase space. For most resonances in our range of temperature, the decay into  $\Lambda(1520) + \pi$  remains weak. The exception is  $\Sigma(1750)$  which decays also to  $\Sigma + \eta$ , see Fig. 7. ( $m_{\Sigma} + m_{\eta} > m_{\Lambda(1520)} + m_{\pi}$ ).  $\Sigma(1750)$  begins to decay dominantly to  $\Lambda^0(1520)$  at relatively low temperature  $T = 116$  MeV, and continues to be produced by  $\Sigma + \eta$  fusion.

As a result, allowing all reactions to go in both directions, the ratio  $\Lambda(1520)/\Lambda(1520)_0$  has a minimum. This is specifically due to  $\Sigma(1750)$  decay back to  $\Lambda(1520)$  at small temperatures as described above. However, when we satisfy Eq. (2) for dead channels the only decay occurs in the beginning of kinetic the dead-channel model phase. In that case the  $\Upsilon_{\Sigma^*}$ s are smaller, and the rate of reaction  $\Lambda(1520) + \pi \rightarrow \Sigma^*$  exceeds the rate for backward reaction by larger amount, compared to the scenario without dead channels. This amplifies the effect of  $\Lambda(1520)$  suppression. In this case,  $\Sigma^*$  decay to lighter hadrons right after they are produced by  $\Lambda(1520)$ . We can see that for  $T_0 = 140$  MeV and  $T_0 = 160$  MeV  $\Lambda(1520)$  yield is always decreasing in the here considered temperature range.

For  $\Sigma(1385)$  multiplicity we find a result quite different from  $\Lambda(1520)$  behavior discussed here, but similar to what we obtained in [9] by a very different method in a smaller basis set of states. In particular, the  $\Sigma(1385)$  yield is enhanced, but the maximum value of  $\Sigma(1385)/\Sigma(1385)_0$  we find is a few percent higher, since we took into account the Bose enhancement of interaction rates, reaction (14), and  $\Sigma^*$  production.  $\Sigma(1385)$  contribution to  $\Sigma^*$  production is small, compared to the influence of the first two effects. The time (i.e. temperature) evolution of  $\Sigma(1385)$  practically does not depend on the presence of dead channels, and the maximum enhancement of  $\Sigma(1385)$  is even less sensitive. This in fact indirectly confirms that  $\Sigma^*$  has a small influence on  $\Sigma(1385)$  multiplicity. Thus we confirm that:

- (i) for  $T_0 = 180$  MeV  $\Sigma(1385)$  evolves with the system following the ambient temperature;
- (ii) for  $T_0 = 160$  MeV  $\Sigma(1385)$  shows some increase in yield;
- (iii) for  $T_0 = 140$  MeV there is a strong yield increase of  $\Sigma(1385)$ .

While there is little sensitivity in the yield of  $\Sigma(1385)$  to issue of particle momentum distribution (little difference

between the two models considered, dashed and solid lines), the  $\Sigma(1385)$  yield is highly sensitive to initial hadronization condition. While for  $\Sigma(1385)$  the yield increases with decreased hadronization temperature, for  $\Lambda(1520)$  the opposite is true, and in particular the smallest final  $\Lambda(1520)$  yield corresponds to the smallest hadronization temperature for both models.

### C. Experimentally measurable resonance ratios

The initial hadronization yields, which we used as a reference in Fig. 6 in order to understand the physical behavior, are not measurable. What is commonly used as a reference for the yields of single strange hyperon resonances is the overall yield of the stable  $\Lambda^0(1115)$ , without the weak decay feed from  $\Xi$ . Aside of the initially produced particles, the experimental yield of  $\Lambda^0(1115)$  also includes resonances decaying during the free expansion after kinetic freeze-out, in particular (nearly) all decays of  $\Sigma(1385)$ , and the experimentally inseparable yield of  $\Sigma^0(1193) \rightarrow \gamma + \Lambda^0$  decay and the decay of any further hyperon resonances  $Y^*$ .

Thus we normalize our final result with the experimentally observable final  $\Lambda_{\text{tot}}^0$  hyperon yield

$$\Lambda_{\text{tot}} = \Sigma^0(1193) + 0.91\Sigma(1385) + \Lambda + Y^*. \quad (42)$$

The factor 0.91 shows that 91% of end-state  $\Sigma(1385)$  decays to  $\Lambda$ . We also included in  $\Lambda_{\text{tot}}$  calculations decays of  $\Xi^* \rightarrow \Lambda + K$ , which makes the result slightly dependent on  $\gamma_s/\gamma_q$  ratio. We use  $\gamma_s/\gamma_q = 1$ , since this ratio value is expected at top RHIC energy [10].

As noted,  $\Lambda(1520)$  and  $\Sigma(1385)$  experimentally observable yields also include any decays which occur in the free-streaming post-kinetic period. Thus we have

$$\Sigma(1385)_{\text{ob}} = \Sigma(1385) + Y_{\Sigma(1385)}^*, \quad (43)$$

$$\Lambda(1520)_{\text{ob}} = \Lambda(1520) + Y_{\Lambda(1520)}^*, \quad (44)$$

where  $Y_{\Sigma(1385)}^*$  and  $Y_{\Lambda(1520)}^*$  are hyperon multiplicities at kinetic freeze-out temperature, and which decay to  $\Sigma(1385)$  and  $\Lambda(1520)$ , respectively. The multiplicities  $\Sigma(1385)$  and  $\Lambda(1520)$  are taken at the moment of kinetic freeze-out.

In Fig. 9 we present the fractional yields  $\Sigma(1385)/\Lambda_{\text{tot}}$  (left), and  $\Lambda(1520)/\Lambda_{\text{tot}}$  (right) as a function of temperature of final kinetic freeze-out  $T$ . The results for the hadronization temperatures  $T_0 = 140$  (blue lines),  $T_0 = 160$  (black lines), and  $T_0 = 180$  MeV (red lines) are shown. Solid lines are for the case with dead channels and dashed lines are for the case when all reactions are going in both directions.

In Fig. 9 the green dash-dotted line is the result when the kinetic freeze-out temperature  $T$  coincides with the

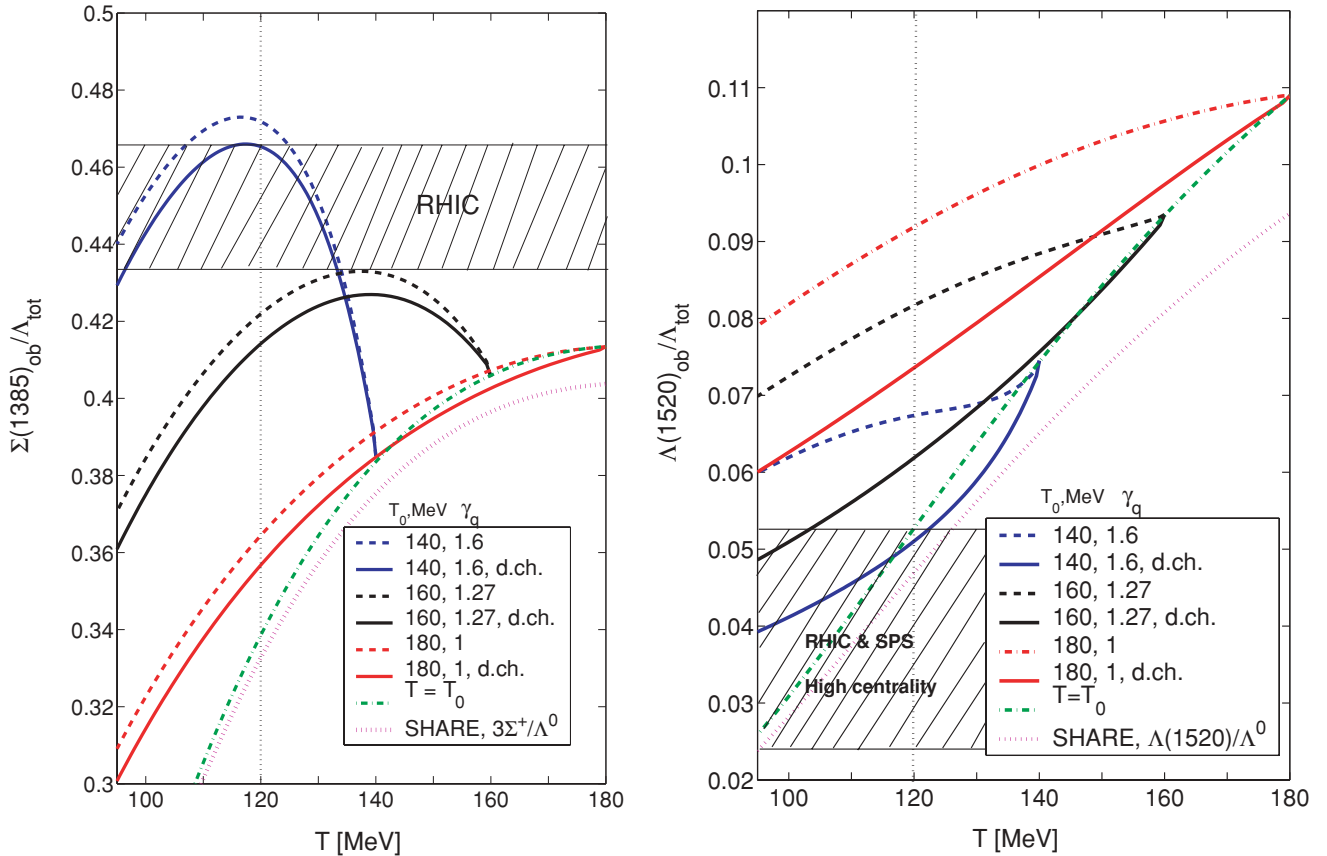


FIG. 9. (Color online) The ratios  $\Sigma(1385)/\Lambda_{\text{tot}}$  (on left) and  $\Lambda(1520)/\Lambda_{\text{tot}}$  (on right) as a function of temperature  $T$  of final kinetic freeze-out, for different initial hadronization temperatures  $T_0 = 140, 160,$  and  $180$  MeV (blue, black, and red lines, respectively). Dashed lines are for calculations without dead channels, solid lines are for calculations with dead channels. The dotted purple line gives the expected SHM chemical equilibrium result. The dash-dot line is relative yield result result for SHM with  $T_0 = T$ .

hadronization temperature  $T_0$ . There is no kinetic phase in this case, only resonances decay after hadronization. This result is similar to SHARE result (purple, dotted line). The small difference is mainly due to us taking into account the decays

$$\Sigma(1670, 1750) \rightarrow \Lambda(1520) + \pi, \quad (45)$$

which are expected/predicted in [16]. Similarly, for  $\Sigma(1385)$  our results for  $T_0 = T$  are different from SHARE results because we include the decay

$$\Sigma(1670) \rightarrow \Sigma(1385) + \pi, \quad (46)$$

expected/predicted in [17]. These additional resonances are part of current particle data set [18].

For all initial hadronization temperatures, as the freeze-out temperature decreases, the suppression for  $\Lambda(1520)_{\text{ob}}/\Lambda_{\text{tot}}$  ratio is larger than for  $\Lambda(1520)/\Lambda(1520)_0$  (at the same temperature  $T$  of final kinetic freeze-out). This is particularly evident for dead channels and hadronization temperatures  $T_0 = 160, 180$  MeV (see Fig. 6). The effect is due to  $\Sigma(1775)$  suppression, as shown in Fig. 8 (and similar for other  $\Sigma^*$ ). For  $T_0 = 140$  MeV the additional suppression of  $\Lambda(1520)$ , described above, is relatively small.

For  $T_0 = 140$  MeV in the case without dead channels at final kinetic freeze-out  $T > 120$  MeV, the final observed  $\Lambda(1520)$  suppression is even smaller, compared to its suppression in the kinetic phase at the same temperature (see Fig. 6). The reason is that yield of  $\Sigma(1775)$  (and of the other  $\Sigma^*$ s) is much enhanced for this range of temperatures see Fig. 8. This additional  $\Sigma(1775)$  decays back to  $\Lambda(1520)$ . That results in a smaller suppression at these temperatures.

The above suppression effect increases in magnitude for higher hadronization temperatures, since the suppression of  $\Sigma(1775)$  and the sensitivity of  $\Lambda(1520)_{\text{ob}}$  multiplicity to  $\Sigma^*$  decays increase with temperature. However, when we consider dead channels (see Fig. 9), the former effect of  $\Lambda(1520)$  suppression during evolution of kinetic phase increases for decreasing hadronization temperatures. Thus in the combined effect, the observable relative suppression of  $\Lambda(1520)_{\text{ob}}/\Lambda_{\text{tot}}$ , is approximately of the same magnitude for all hadronization temperatures  $T_0$ . However, the initial hadronization yield of  $\Lambda(1520)$  is sensitive to temperature, and decreases rapidly with  $T$ . Therefore only for  $T_0 = 140$  MeV, a kinetic freeze-out temperatures  $\approx 95\text{--}105$  MeV, and allowing for dead channels, the ratio  $\Lambda_{\text{ob}}(1520)/\Lambda_{\text{tot}}$  reaches the experimental domain  $\Lambda_{\text{ob}}(1520)/\Lambda_{\text{tot}} < 0.042 \pm 0.01$  [1,2] shown in Fig. 9 by dashed lines.

For the same initial conditions, that is for  $T_0 = 140$  MeV, we find the ratio  $\Sigma(1385)/\Lambda_{\text{tot}} \approx 0.45$  at  $T \approx 100$  MeV (and for the entire range 95–135 MeV, in good agreement with experimental data [2,3]). In [9] this value of  $\Sigma(1385)/\Lambda_{\text{tot}}$  is found at  $T = 120$  MeV, which was in the reference the presumed lowest possible temperature of the final kinetic freeze-out. Here we find that at  $T = 120$  MeV the ratio  $\Sigma(1385)/\Lambda_{\text{tot}}$  can be even higher (about 0.47), which is due to the Bose enhancement of in-medium  $\Sigma(1385)$  production rate (see discussion following Fig. 6).

#### IV. CONCLUSIONS

The resonant hadron states, considering their very large decay and reaction rates, can interact beyond the chemical and thermal freeze-out of stable particles. Thus the observed yield of resonances is fixed by the physical conditions prevailing at a later breakup of the fireball matter rather than the production of nonresonantly interacting hadrons. Moreover, resonances, observed in terms of the invariant mass signature, are only visible when emerging from a more dilute hadron system given the ample potential for rescattering of decay products. The combination of experimental invariant mass method with a large resonant scattering makes the here presented population study of resonance kinetic freeze-out necessary. The evolution effects we find are greatly amplified at low hadronization temperatures where greatest degree of initial chemical equilibrium is present.

Our study quantifies the expectation that in a dense hadron medium narrow resonances are “quenched” [7] that is, effectively mixed with other states, and thus their observed population is reduced. Since we follow here the particle density, the effect we study is due to incoherent population mixing of  $\Lambda(1520)$ , in particular with  $\Sigma^*$ . This effect is possible for particle densities out of chemical nonequilibrium. However, this mixing can occur also at the amplitude (quantum coherent) level. As the result the yield suppression effect could further increase, in some situations further improving the agreement with experiment.

Our results show that the observable ratio  $\Lambda(1520)_{\text{ob}}/\Lambda_{\text{tot}}$  can be suppressed by two effects. First  $\Lambda(1520)$  yield is suppressed due to excitation of heavy  $\Sigma^*$ s in the resonance scattering process. Moreover, the final  $\Lambda(1520)_{\text{ob}}$  yield is suppressed, because  $\Sigma^*$ s, which decay to  $\Lambda(1520)$ , are suppressed at the end of the kinetic phase evolution by their (asymmetric) decays to lower mass hadrons, especially when dead channels are present (see Fig. 8). As a result, fewer of these hadrons can decay to  $\Lambda(1520)_{\text{ob}}$  during the following free expansion. A contrary mechanism operates for the resonances such as  $\Sigma(1385)$ ,  $\Delta(1230)$ . These resonances can be so strongly enhanced, that in essence most final states strange and non-strange baryons come from a resonance decay.

We note that despite a scenario dependent resonance formation or suppression, the stable particle yields used in study of chemical freeze-out remain unchanged, since all resonances ultimately decay into the lowest “stable” hadron. Therefore after a description, e.g., within a statistical hadronization model of the yields of stable hadrons, the understanding of resonance yields is a second, and separate task which helps to establish the consistency of our physical understanding of the hadron production process.

We conclude noting the key result of this study, that we can now understand the opposite behavior of  $\Lambda(1520)$  (suppression in high centrality reactions) and  $\Sigma(1385)$  [enhancement, and similarly  $\Delta(1230)$ ] by considering their rescattering in matter. In order to explain both, the behavior of the  $\Lambda(1520)_{\text{ob}}/\Lambda_{\text{tot}}$  and  $\Sigma(1385)/\Lambda_{\text{tot}}$  ratios, one has to consider  $T = 95\text{--}100$  MeV as the favorite temperature of final kinetic freeze-out of hadron resonances, with  $T_0 = 140$  MeV being the favored chemical freeze-out (hadronization, QGP break-up) temperature. When there is little matter available to scatter, e.g.,

in peripheral collisions, the average value of  $\Lambda(1520)_{\text{ob}}/\Lambda_{\text{tot}}$  ratio is higher, approaching the expected chemical freeze-out hadronization yield for  $T_0 = 140$  MeV. All these findings are in good agreement with available experimental data.

#### ACKNOWLEDGMENTS

This research was supported by a grant from the US Department of Energy DE-FG02-04ER4131 and by the DFG-LMU Excellent program.

- 
- [1] C. Markert (STAR Collaboration), *J. Phys. G* **28**, 1753 (2002).
  - [2] J. Adams *et al.* (STAR Collaboration), *Phys. Rev. Lett.* **97**, 132301 (2006).
  - [3] S. Salur, *J. Phys. G* **32**, S469 (2006).
  - [4] C. Markert (STAR Collaboration), *J. Phys. G* **35**, 044029 (2008).
  - [5] R. Witt, *J. Phys. G* **34**, S921 (2007).
  - [6] B. I. Abelev *et al.* (STAR Collaboration), *Phys. Rev. C* **78**, 044906 (2008).
  - [7] J. Rafelski, J. Letessier, and G. Torrieri, *Phys. Rev. C* **64**, 054907 (2001) [Erratum-*ibid.* **65**, 069902 (2002)]; G. Torrieri and J. Rafelski, *Phys. Lett.* **B509**, 239 (2001); *Phys. Rev. C* **68**, 034912 (2003).
  - [8] M. Bleicher and J. Aichelin, *Phys. Lett.* **B530**, 81 (2002); M. Bleicher and H. Stoecker, *J. Phys. G* **30**, S111 (2004); S. Vogel and M. Bleicher, Proceedings of the 22nd Winter Workshop on Nuclear Dynamics, La Jolla, CA, 11–19 March, 2006, arXiv:hep-ph/0607242.
  - [9] I. Kuznetsova and J. Rafelski, *Phys. Lett.* **B668**, 105 (2008).
  - [10] I. Kuznetsova and J. Rafelski, *Eur. Phys. J. C* **51**, 113 (2007).
  - [11] I. Kuznetsova, T. Kodama, and J. Rafelski, “Chemical Equilibration Involving Decaying Particles at Finite Temperature” (in preparation).
  - [12] I. Kuznetsova, D. Habs, and J. Rafelski, *Phys. Rev. D* **78**, 014027 (2008).
  - [13] G. Torrieri, S. Steinke, W. Broniowski, W. Florkowski, J. Letessier, and J. Rafelski, *Comput. Phys. Commun.* **167**, 229 (2005).
  - [14] G. Torrieri, S. Jeon, J. Letessier, and J. Rafelski, *Comput. Phys. Commun.* **175**, 635 (2006).
  - [15] J. Letessier and J. Rafelski, *Phys. Rev. C* **75**, 014905 (2007).
  - [16] W. Cameron *et al.* (Rutherford-London Collaboration), *Nucl. Phys.* **B131**, 399 (1977).
  - [17] J. Prevost *et al.* (Cern-Heidelberg-Saclay Collaboration), *Nucl. Phys.* **B69**, 246 (1974).
  - [18] C. Amsler *et al.* (Particle Data Group), *Phys. Lett.* **B667**, 1 (2008).